Energy Storage Materials 51 (2022) 391–399

Contents lists available at ScienceDirect

Energy Storage Materials

journal homepage: www.elsevier.com/locate/ensm

Molecularly engineered three-dimensional covalent organic framework protection films for highly stable zinc anodes in aqueous electrolyte

Kuan Wu [a,1], Xiansong Shi [c,1], Fangfang Yu [b], Haoxuan Liu [b], Yuanjun Zhang [a], Minghong Wu [a], Hua-Kun Liu [b], Shi-Xue Dou [b], Yong Wang [c], Chao Wu [a,b,*]

[a] School of Environmental and Chemical Engineering, Shanghai University, Shanghai 200444, China
[b] Institute for Superconducting & Electronic Materials, Australian Institute of Innovative Materials, University of Wollongong, NSW 2522, Australia
[c] State Key Laboratory of Materials-Oriented Chemical Engineering, College of Chemical Engineering, Nanjing Tech University, Nanjing 211816, Jiangsu, PR China

ARTICLE INFO

Keywords:
Covalent organic frameworks
Zn anode
Aqueous electrolyte
Protective film
Zn dendrites

ABSTRACT

Metallic Zn has been regarded as ideal anodes in aqueous electrolyte owing to its high theoretical capacity, intrinsic safety, low cost, and nontoxicity. However, the Zn dendrite growth and the side-reactions hindered the practical application of Zn anode. Herein, a thin and uniform three-dimensional (3D) COOH-functionalized covalent organic frameworks (COF) film (denoted as 3D-COOH-COF) is designed and *in-situ* synthesized as a protective layer to stabilize the Zn anode. The thin 3D-COOH-COF protection film with abundant negative functional groups and homogeneous nanochannels facilitates the fast transport of Zn^{2+}, impedes the pass through of SO_4^{2-}, and significantly suppresses the corrosion reactions, leading to an excellent electrochemical performance. The novel 3D-COOH-COF protective film enables the Zn||Zn symmetric cells to stably cycle for over 2000 h at 1 mA cm^{-2} and an average Coulombic efficiency of Zn plating/stripping as high as 99.5% for 1000 cycles at 1 mA cm^{-2}.This finding provides a facile and promising route to regulate the deposition behavior of Zn in aqueous electrolyte.

1. Introduction

The development of grid energy storage as sparked an ever-increasing interest in investigating alternative energy storage technologies to Li-ion batteries owing to their safety issues and high cost [1,2]. Aqueous rechargeable batteries, which are based on safe and low-cost water-based electrolytes, have been regarded as one of the most promising candidates for grid energy storage. As for the anode choice of aqueous batteries, metallic zinc (Zn) has attracted tremendous attention as anode owing to its low cost, high theoretical capacity (820 mA h g^{-1}), and low potential (−0.762 V versus the standard hydrogen electrodes) [3–8]. However, Zn anodes suffer from a few challenging issues such as the poor reversibility and the growth of Zn dendrites in neutral aqueous solutions which not only shorten the lifespan of batteries but also bring the safety concerns [5–10].

Recently, a variety of strategies have been developed to stabilize the Zn anode, such as the constructing the nucleation layer or skeletons [10,11], optimizing the electrolytes or additives [12–16], and creating the surface protective layers [17–23]. Among these strategies, the creation of protective layer offers a facile and promising route to guide the uniform Zn deposition. Although the reported protective layers can modify the electrochemical performance of Zn, there are still some problems in the design of the protective film. First, most of the reported films are constructed by coating functional inorganic/organic fillers mixed with the polymer binder on the Zn foil [24,25]. These fillers were coated on the Zn foil by the polymer binder, and the distribution of fillers is easy to be inhomogeous. Additionally, the size and distribution of pores between fillers are also nonuniform, which affect Zn^{2+} to uniformly pass through the protective layer homogeneously. Finally, the reported polymer composite film generally shows a single function and cannot block the anions to pass through the protective film, which cannot suppress the side reactions that anoions take part in on the Zn surface [4]. Therefore, rational design and construction of protective films on the Zn anode is essential to overcome the above problems, which remains a challenge.

As an emerging versatile material, covalent organic frameworks

* Corresponding author at: School of Environmental and Chemical Engineering, Shanghai University, Shanghai 200444, China.
E-mail address: chaowu@uow.edu.au (C. Wu).
[1] These authors contributed equally to this work.

https://doi.org/10.1016/j.ensm.2022.06.032
Received 14 April 2022; Received in revised form 10 June 2022; Accepted 20 June 2022
Available online 21 June 2022

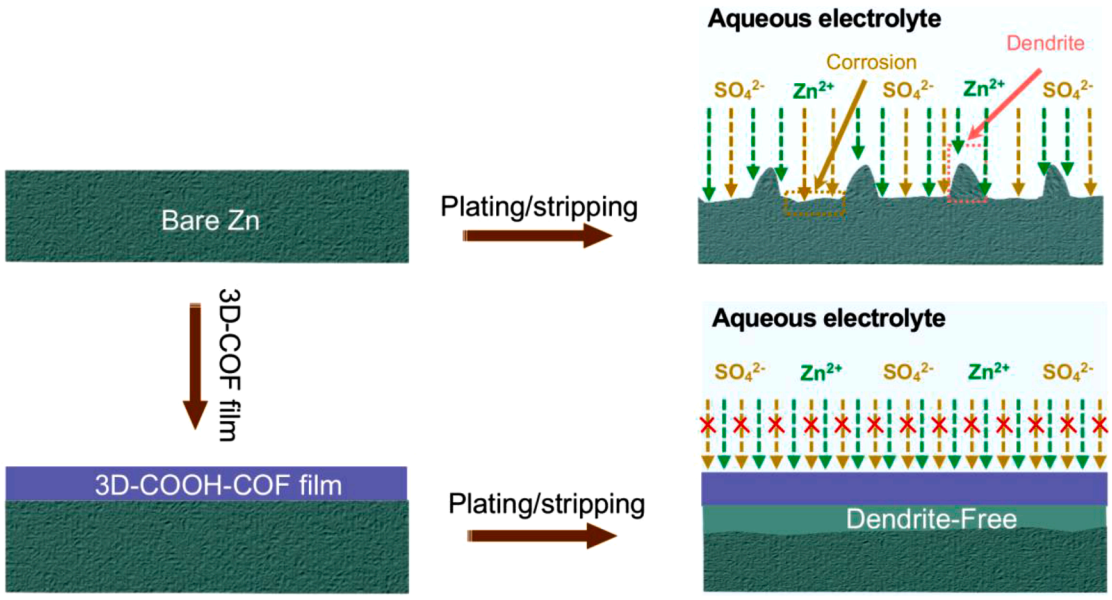

Fig. 1. Schematic illustration of the Zn deposition behavior on the bare Zn and 3D-COOH—COF@Zn.

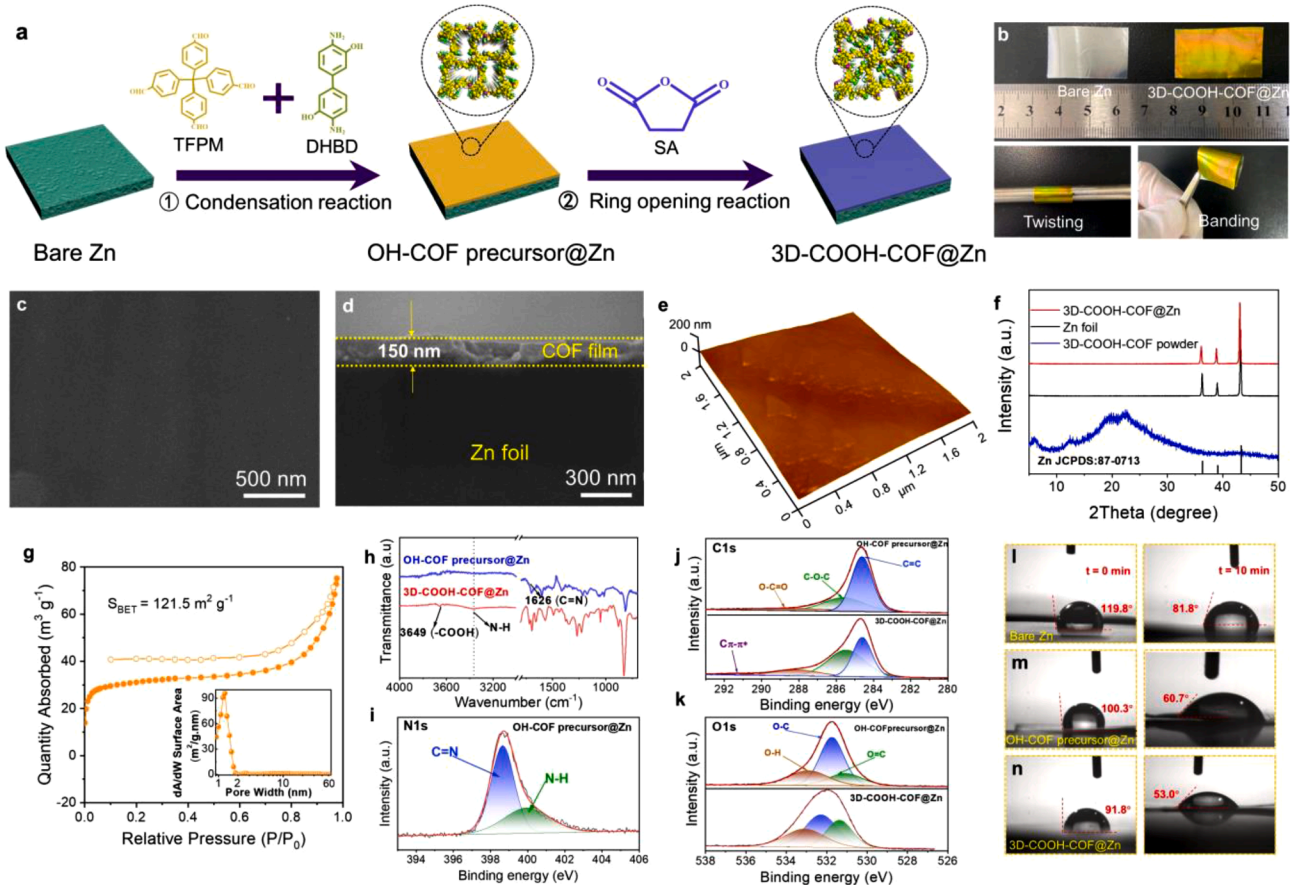

Fig. 2. (a) Schematic illustration of synthesis of OH—COF precursor@Zn and 3D-COOH—COF@Zn. (b) Optical photos of bare Zn and 3D-COOH—COF@Zn. (c) Top-view and (d) cross-sectional SEM images of 3D-COOH—COF@Zn. (e) AFM image of 3D-COOH—COF@Zn. (f) XRD patterns of bare Zn, 3D-COOH—COF@Zn, and 3D-COOH—COF powder. (g) BET measurement and pore size distribution (inset) of 3D-COOH—COF@Zn. (h) FTIR spectra of OH—COF precursor@Zn and 3D-COOH—COF@Zn. (i) N1s spectrum of OH—COF precursor@Zn. (j) C1s and (k) O1s spectra of OH—COF precursor@Zn and 3D-COOH—COF@Zn. (l–n) The contact angles of aqueous electrolyte on the bare Zn (l), OH—COF precursor@Zn (m), and 3D-COOH—COF@Zn (n).

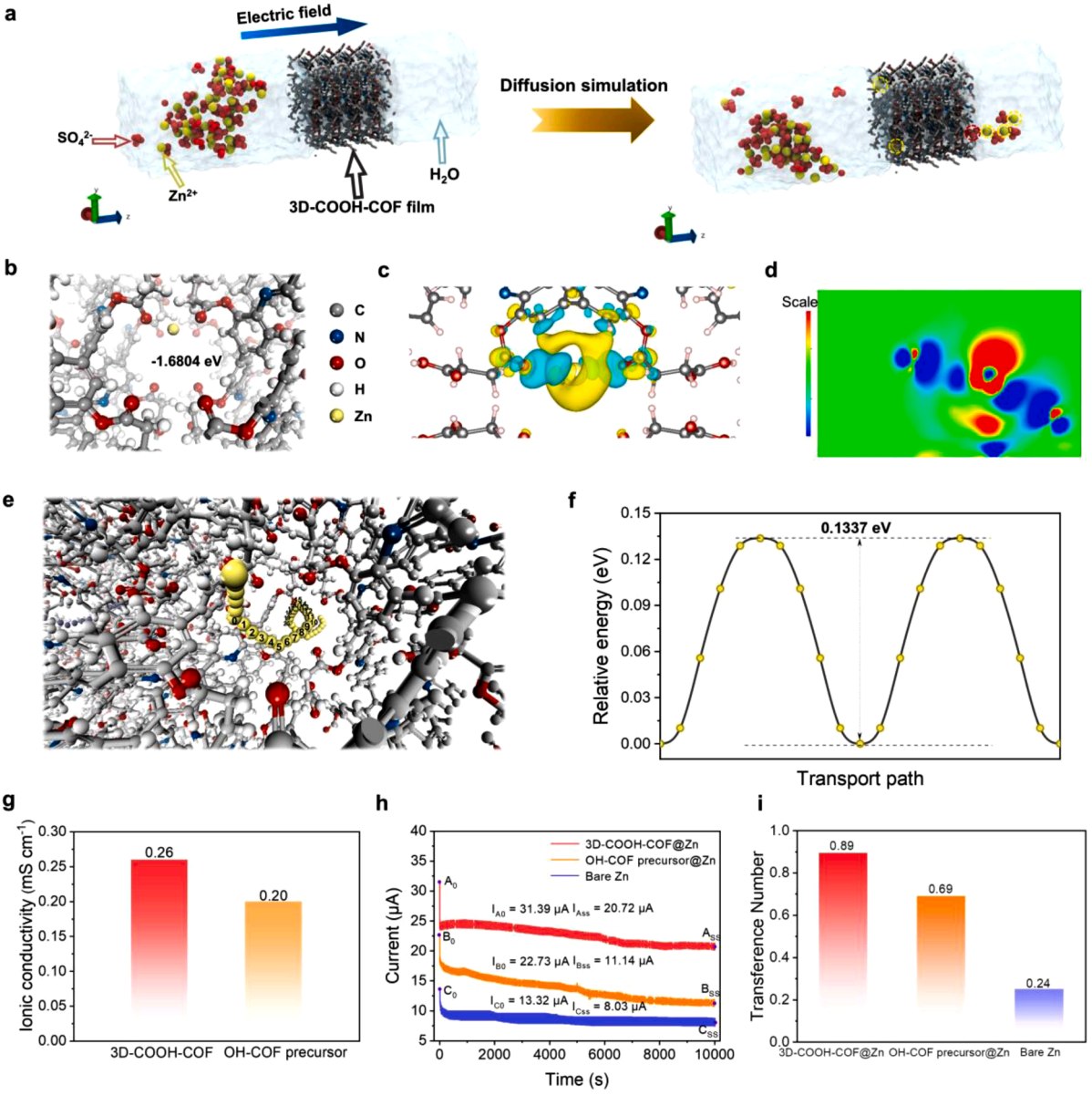

Fig. 3. (a) Molecular Dynamics Simulations of Zn^{2+} and $SO4^{2-}$ ions to pass through the 3D-COOH—COF film (b) The calculated binding energy of Zn^{2+} on the 3D-COOH—COF. (c) Electron density difference map of the 3D-COOH—COF with Zn^{2+}adsorption and (d) the corresponding sliced 2D contour map. (e) The optimized Zn-ion diffusion pathway in the 3D-COOH—COF layer and (f) the correponding migration energy barrier. (g) Ionic conductivity of OH—COF precursor@Zn and 3D-COOH—COF@Zn. (h) Current variations of bare Zn, OH—COF precursor@Zn, and 3D-COOH—COF@Zn in symmetric cell with a potentiostatic polarization. (i) The Zn^{2+} transference number in the cells using bare Zn, OH—COF precursor@Zn, and 3D-COOH—COF@Zn electrodes. The whole system is in zinc sulfate aqueous solution.To show clearly, water molecules are expressed in transparent color without direct marking.

(COFs) have received tremendous attention due to their designable structures and extremely ordered mass transfer channels. By deeply exerting these distinctive advantages, COFs have shown great potentials in a variety of advanced applications, such as sensing, separation, energy storage and conversion [26–28]. Owing to the nano-sized aperture sizes and prominent porosities, COFs potentially allow the fast and exclusive transport of metal ions, benefiting the performance improvement during charge and discharge cycles. In addition, the post-synthetic modification promises the precise engineering of COF pore wall environments for on-demand purposes, in favor of devising specific functions without compromising structural stability and uniformity. Moreover, as a sub-family of COFs, three-dimensional (3D) COFs constructed by reticular chemistry can provide interconnected channels, which potentially benefit for the promotion of ion transport. Thus, the molecular engineering of COFs has huge potential to construct novel protective layers to obtain high-performance and stable Zn anode.

Here, we have designed and *in-situ* synthesized a ultrathin and uniform three-dimensional (3D) COOH-functionalized covalent organic frameworks (COF) film (denoted as 3D-COOH-COF) with high mechanical strength to protect the Zn anodes. This unique and novel 3D-COOH-COF protective layer provides a variety of advantages. First, a thin thickness and uniform nanochannels of COF layer facilitate the fast and homogeneously transport of Zn^{2+} around the surface of Zn anode. Second, abundant negative COOH-functionalized groups of 3D skeleton and nanochannels of the COF film impede sulfate ions to pass through the protective film, resulting a high transfer number of Zn^{2+} and dendrite-free deposition of Zn metal. Third, the 3D-COOH-COF film can uniformly and fully cover the current collectors and Zn anodes without any gaps, effectively prevent the direct contact between Zn anode and aqueous electrolyte, and significantly suppress the corrosion reactions.

Such advantages of 3D-COOH-COF film can not only reduce side reaction through selectively accelerating Zn^{2+} and inhibiting anions transport, but also suppress dendrite growth by ensuring even Zn^{2+} plating/stripping (Fig. 1). Consequently, Zn-ion batteries based on Zn anodes with 3D-COOH-COF layers exhibit excellent electrochemical performance.

2. Results and discussions

The fabrication process of 3D-COOH—COF film coated on the Zn foil is illustrated in Fig. 2a, which involves two major steps. First, -OH functionalized 3D-OH—COF precursor film was synthesized on the Zn foil by *in-situ* growth method [26,27]. The thickness and surface flatness are dependent on the concentration of tetra(4-formylphenyl) methane (TFPM) and 3,3′-dihydroxybenzidine (DHBD), as shown in Fig. S1. Scanning electron microscopy (SEM) images reveal that the prepared OH—COF precursor film is densely loaded on the Zn foil with a smooth surface at the concentration of 1.08 mg mL^{-1} (Fig. S1d–f). Additionally, the photos show that the obvious color changes (insets of Fig. S1) under different concentrations of TFPM and DHBD. Subsequently, the OH—COF precursor film was further funtionlized to achieve the -COOH functionalized 3D-COOH—COF film coated on the Zn foil (denoted as 3D-COOH—COF@Zn) through post-synthetic modification @Zn. It should be mentioned that the obtained film has an excellent chemical stability in aqueous solution in our previous study [26]. The 3D-COOH—COF film with a microporous structure and hydrophilic functional groups (Fig. S2) could provide high ionic conductivity and good hydrophilic property [22]. Moreover, the 3D-COOH—COF film shows good adhesion to the Zn foil and did not peer off even under the twisting and bending state (Fig. 2b). The top-view SEM image reveals a dense and uniform 3D-COOH—COF film with a thickness of ~150 nm on the Zn foil (Figs. 2c, d and S3a). Moreover, energy dispersive spectroscopy (EDS) mapping images display that C, O, and N elements are homogeneously distributed on the surface, indicating the excellent integrity of 3D-COOH—COF (Fig. S4). Atomic force microscopy (AFM) image shows that the Zn foil is evenly and homogeneously covered by 3D-COOH—COF film (Fig. 2e). It should be noted that the surface morphology of 3D-COOH—COF film is related to the concentrations of TFPM and DHBD. 3D-COOH—COF film shows great unevenness on the Zn foil at the concentration of 0.51, 2.05, and 3.07 mg mL^{-1}, which is confirmed by the result of AFM (Fig. S5).

The 3D-COOH—COF film were further investigated by X-ray diffraction (XRD) and Brunauer-Emmett-Teller (BET). 3D-COOH—COF@Zn shows the same XRD diffraction peaks with the Zn foil (PDF# 87–0713) without the phase of 3D-COOH—COF, which is attributed to the thin thickness of the COF protective film (Fig. 2f) [29]. From the XRD pattern of the powder generated during film synthesis (Fig. S3b, c), we can observe the diffraction signals corresponding to crystalline 3D-COOH—COF. This reflects the crystallinity of films as they are concurrently generated under the same solvothermal conditions. BET measurement reveals the surface area of the 3D-COOH—COF film (Fig. 2g) is up to 121 $m^2\ g^{-1}$, higher than that of OH—COF precursor film (107.4 $m^2\ g^{-1}$), which is shown in Fig. S6. The centered pore size distribution of 3D-COOH—COF film is at 1.3 nm in diameter compared with OH—COF precursor film (~1.6 nm), indicating that the modification of functional groups has little effect on the specific surface and pore size distribution. Fig. 2h shows Fourier transform infrared (FT-IR) spectrum of 3D-COOH—COF@Zn. The characteristic absorption band of C = N (1626 cm^{-1}) displayed the presence of imine linkages of 3D-COOH—COF in the protection film. The absorption peak of 3D-COOH—COF@Zn at 3649 cm^{-1} originates from the COOH bond [19,30]. High-resolution X-ray photoelectron spectroscopy (XPS) displays that the N1s spectra have the weak peak at 399.91 eV, corresponding to the N—H bond (Fig. 2i), indicating that COF films contain a small amount of residual amino groups, consistent with the FTIR result [30]. The conversion of OH—COF precursor@Zn to 3D-COOH—COF@Zn can also be confirmed by XPS analysis. Compared to the OH—COF precursor, the peak intensity of O—C = O (288.4 eV) and C = O (530.9 eV) in the C1s and O1s spectra of 3D-COOH—COF@Zn (Fig. 2j, k) are increased, suggesting the successful linkage of COOH functional groups on the COF skeletons [27,31]. The hydrophilicity of 3D-COOH—COF@Zn for the electrolytes (2 M $ZnSO_4$) was estimated by the contact angle test at ambient temperature (Fig. 2l–n). After 10 min, the contact angle of the bare Zn is still found to be 81.8°, indicating the limited hydrophilicity of the Zn surface (Fig. 2l). In contrast, the contact angles of OH—COF precursor and 3D-COOH—COF films are smaller than that of the bare Zn, indicating that the 3D-COOH—COF protective films enhance the hydrophilicity owing to their rich functional groups. It is worth noting that the hydrophilicity of 3D-COOH—COF film is superior to OH—COF precursor because of its rich carboxyl groups on the COF skeleton. The interfacial free energy at the electrode/electrolyte interface will be reduced as the hydrophilicity enhances [22,32] which is beneficial for Zn nucleation and uniform Zn deposition.

3D-COOH—COF protective film allows for the fast transport of Zn^{2+} and hinders the transport of sulfate ions because of its unique structure and rich COOH functional groups. Molecular Dynamics Simulations (MDS) was used to investigate the Zn^{2+} and SO_4^{2-} anion transport behavior to pass through the 3D-COOH—COF protective film in 2 M $ZnSO_4$ solution. Before the simulation, cation and anion ions were set at one side of this 3D-COOH—COF film. After a period of time, it was obvious that zinc ions can pass through the 3D-COOH—COF film while sulfate ions were blocked because of COOH-rich electronegative skeleton and microporous channel of 3D-COOH—COF (Fig. 3a), which could also be seen in the simulated trajectory diagram of MDS (Video 1). To further understand the role of the 3D-COOH—COF film for the Zn protection, density functional theory (DFT) calculations were carried out. The calculated models of the interaction between Zn^{2+} and 3D-COOH—COF are displayed in Fig. 3b. The 3D-COOH—COF layer has a strong adsorption with Zn^{2+}, with a binding energy of −1.6804 eV, indicating the electrostatic interaction between Zn^{2+} and the 3D-COOH—COF layer [33–36]. Fig. 3c, d show differential charge density and the corresponding sliced 2D contour map for 3D-COOH—COF with Zn^{2+}adsorption, indicating that the 3D-COOH—COF layer can adhere Zn^{2+} to increase the local Zn^{2+} around the surface Zn foil and reduce the concentration gradient at the interface. This feature is beneficial to inhibit the zinc dendrite growth.

To further explore the transport behavior of Zn^{2+} to pass through the 3D-COOH—COF film, the diffusion channel in the 3D-COOH—COF film was simulated, as shown in Fig. 3e and 3f. It shows that the zinc ion diffusion energy barrier under this optimized pathway is 0.1337 eV, which is lower than thant of preveiouly reported Zn or Zn-ion aqueous batteries (Table S1), further indicating that 3D-COOH—COF protection film can facilitate the transport of Zn^{2+} and homogenize the distribution of Zn^{2+} [34,37–40] As shown in Figs. 3g and S7, the 3D-COOH—COF film presents a high ionic conductivity, which is higher than that of OH—COF precursor film. In addition to ionic conductivity, Zn^{2+} transference number (t^+) was measured, and the specific equation is given in Supporting Information (Fig. S8) [20,40]. The initial currents (I_0) and the steady-state current (I_{ss}) after potentiostatic polarization for 10000s were shown in Fig. 3h. As shown in Fig. 3i, the Zn-ion transference number (t_{zn}^{2+}) of 3D-COOH—COF@Zn electrode is as high as 0.82, which was higher than that of OH—COF precursor@Zn electrode (0.69), indicating the faster Zn^{2+} cation than $SO4^{2-}$ anion in the 3D-COOH—COF film. In contrast, for the bare Zn electrode, the t_{zn}^{2+} is only 0.24. According to the study of Rosso et al. [41], the larger transference number of cations can inhibit the growth of Zn dendrite. The high Zn^{2+} transfer number is attributed to a strong electronegative functional group, which is confirmed by Zeta potential curves. These functional groups can adsorb Zn^{2+} well and have a good blocking effect on anions (Fig. S9). These results illustrate that the protective layer can effectively promote the rapid transport of Zn^{2+} and prevent the anion transport, suppressing the generation of Zn dendrites, which is

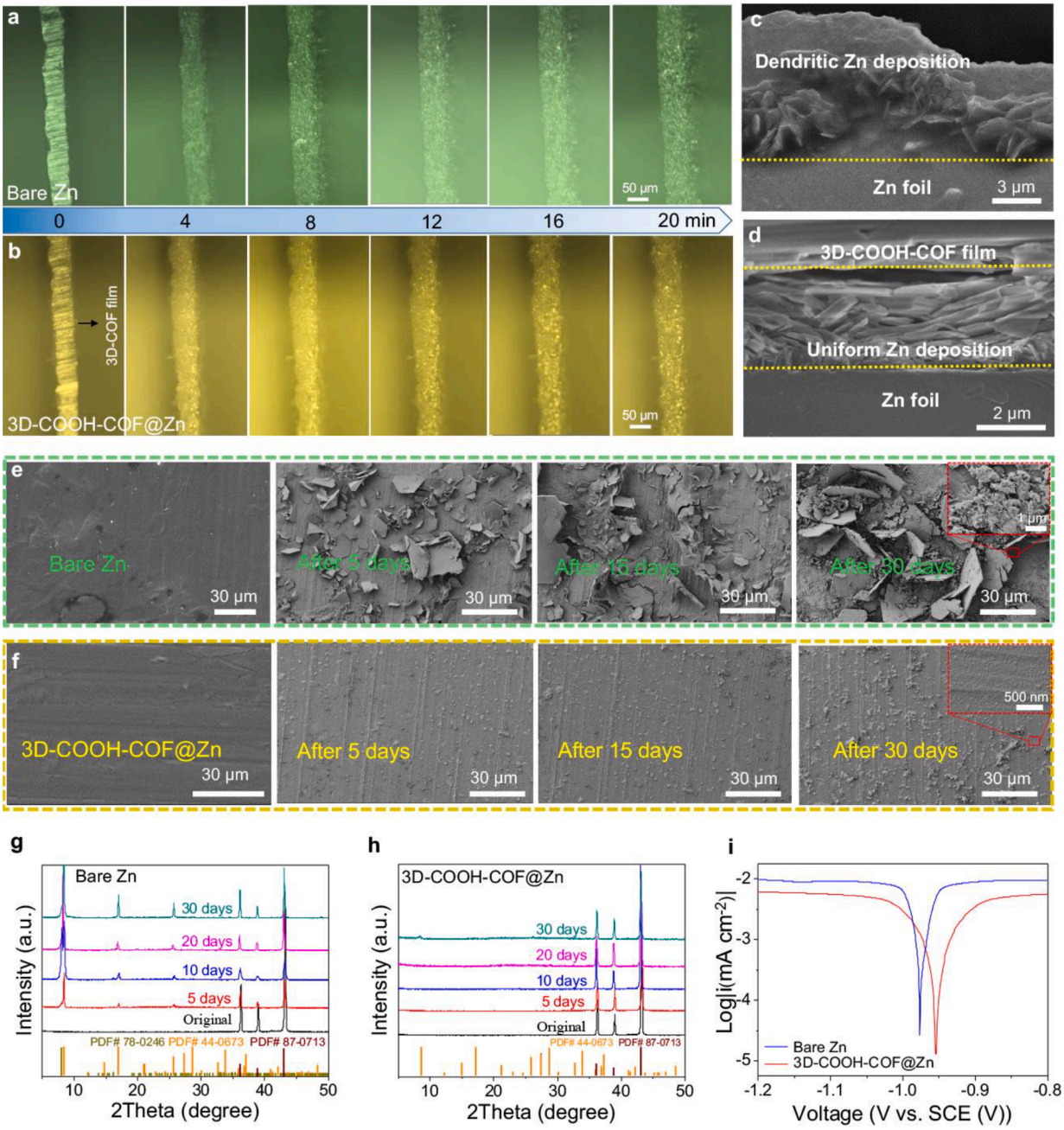

Fig. 4. (a, b) The *in-situ* optical microscopy images of bare Zn (a) and 3D-COOH—COF@Zn (b) electrode recorded at the specified deposition time at 3 mA cm^{-2}. (c, d) Cross-seactional SEM images of bare Zn (c) and 3D-COOH—COF@Zn (d) at 1 mA cm^{-2} for 1 h. (e, f) SEM images of (e) bare Zn and (f) 3D-COOH—COF@Zn after being soaked for 5 days, 15 days, and 30 days, respectively. (g, h) XRD patterns of (g) bare Zn and (h) 3D-COOH—COF@Zn after different days. (i) Linear polarization curves of bare Zn and 3D-COOH—COF@Zn.

consistent with the simulation results.

3D-COOH—COF protective film shows excellent kinetics of Zn^{2+} and homogenize the Zn^{2+} distribution around the Zn foil, which inhibits the growth of Zn dendrites. To visually observe the electrodeposition behavior of Zn metal underneath the 3D-COOH—COF film, the Zn plating process was monitored through *in-situ* optical microscope. As shown in Fig. 4a, some zinc protuberances with a random distribution can be visible on the bare Zn foil after electrodeposition for 8 min. As the plating time increases to 20 min, the protrusions continuously grew and the zinc dendrites could be obviously observed. By contrast, for 3D-COOH—COF protected Zn foil, a smooth surface morphology was presented over the whole deposition process, and no obvious dendrites were detected (Fig. 4b), verifying the uniform Zn electrodeposition behavior under the 3D-COOH—COF protective film. The scanning electron microscopy (SEM) images reveal that the Zn deposition located under the 3D-COOH—COF protection layer is dense (Fig. 4c, d) and the surface is also smooth (Fig. S10) .

The COF protective layer not only promotes the homogenous deposition of Zn, but also significantly reduces the corrosion between aqueous electrolyte and Zn foil. To study the anti-corrosion effect of the 3D-COOH—COF protective layer, Zn foils covered without and with the 3D-COOH—COF film were soaked into an aqueous electrolyte (2 M $ZnSO_4$ solution) (Fig. S11a). As shown in the SEM images (Fig. 4e), obvious chemical-corrosion products appeared on the surface of Zn foil after 5 days. As the soaking time increases, more by-products were detected along with the interfacial side reactions. In striking contrast,

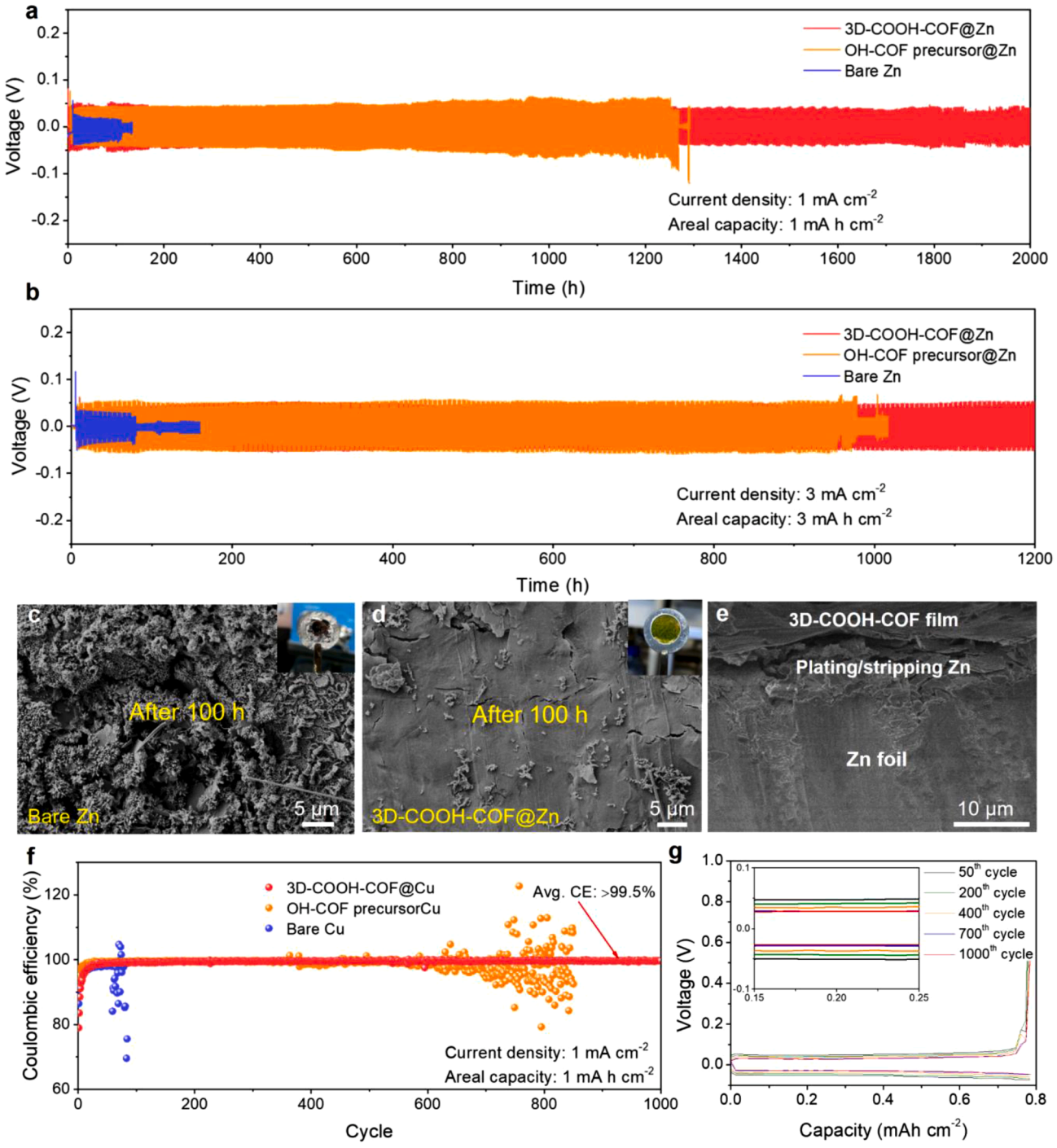

Fig. 5. (a, b) Long-term cycling performance of Zn plating/stripping in symmetrical cells based on bare Zn, OH—COF precursor@Zn, and 3D-COOH—COF@Zn at 1 mA cm^{-2} and 1 mA h cm^{-2} (a) as well as 3 mA cm^{-2} and 3 mA h cm^{-2} (b). Top-view SEM images of bare Zn (c) and 3D-COOH—COF@Zn electrode (d), and cross-sectional SEM image of 3D-COOH—COF@Zn electrode (e) after 100 h at 1 mA cm^{-2} and 1 mA h cm^{-2}, the insets show the photos of the cycled electrodes. (f) CE of Zn plating/stripping on bare Cu, OH—COF precursor@Cu, and 3D-COOH—COF@Cu at 1 mA cm^{-2} and (g) the corresponding voltage profiles at various cycles on 3D-COOH—COF@Cu.

even after soaked for 30 days, the 3D-COOH—COF film was still maintained, with a flat surface (Fig. 4f). Bare Zn and 3D-COOH—COF@Zn were further examined after being soaked for 100 days. The Zn plate turned completely gray and 3D-COOH—COF@Zn remained lustrous (Fig. S11b, c). These results demonstrate the excellent chemical stability of 3D-COOH—COF@Zn against to the electrolyte. Moreover, XRD spectra were used to identify the surface composition of Zn foil without and with the COF protective film after different soaking time (Fig. 4g, h). For the bare Zn foil, a few new peaks are found, corresponding to $Zn_4SO_4(OH)_6{\cdot}5H_2O$ (PDF# 78–0246) and $Zn_4SO_4(OH)_6{\cdot}4H_2O$ (PDF# 44–0673) [22,30]. Additionally, as soaking time increases, the intensity of these peaks become stronger (Fig. 4g), further confirming the increased corrosion reactions. For 3D-COOH—COF protected Zn foil, no new peaks were generated (Fig. 4h), which is consistent with the result of SEM. The anti-corrosion effect of the COF protective film was investigated by linear polarization experiment in 2 M $ZnSO_4$ electrolyte.

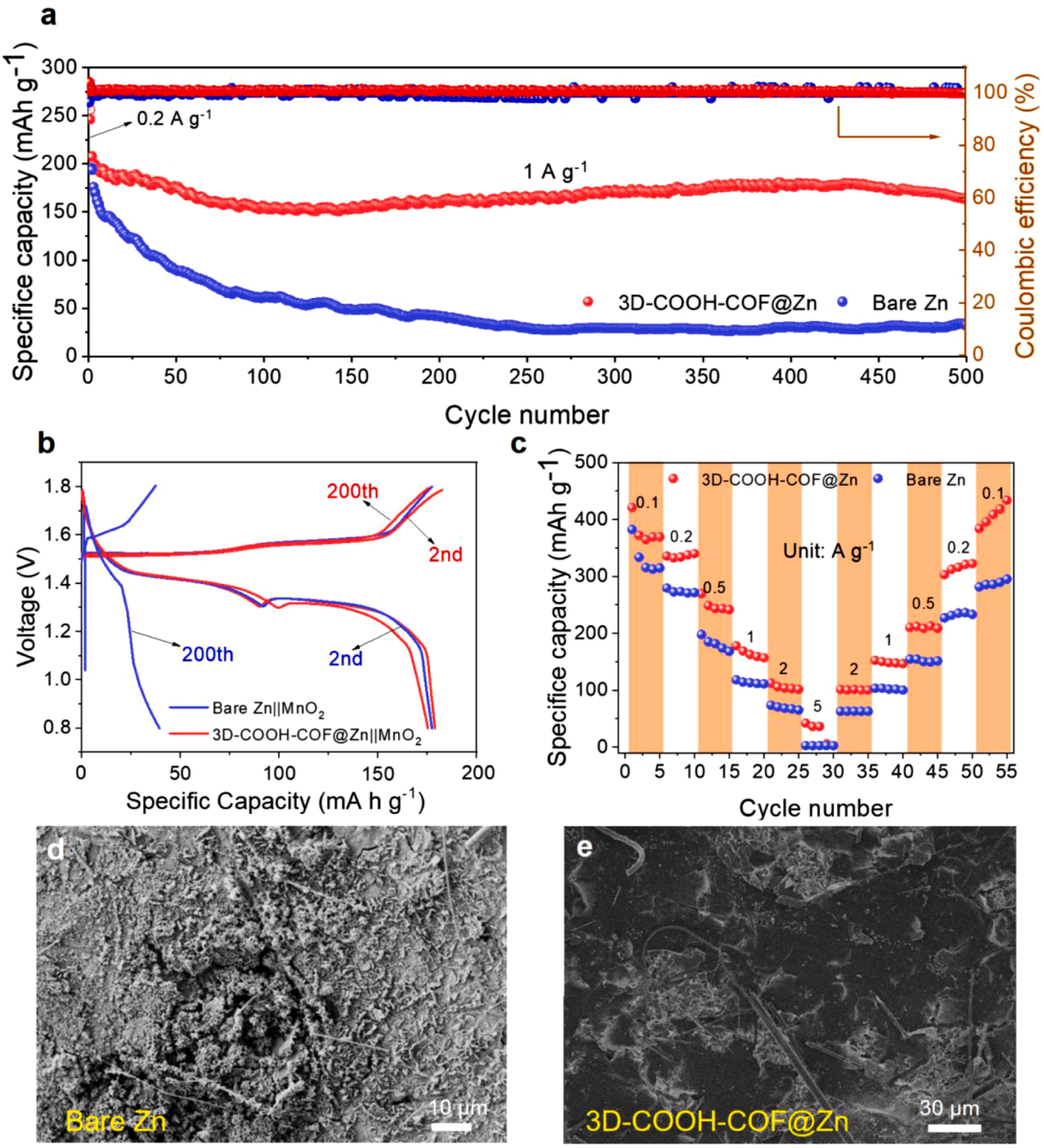

Fig. 6. The electrochemical performance of bare Zn||MnO_2 and 3D-COOH—COF@Zn||MnO_2 cell: (a, b) long-term cycling stability and efficiency (a) and galvanostatic charge/discharge curves (b) at 1 A g^{-1}, (c) rate capability, and (d, e) SEM images of the bare Zn anode (d) and the 3D-COOH—COF@Zn anode after 500 cycles (e).

Compared to the bare Zn foil, the corrosion potential of the 3D-COOH—COF@Zn electrode increased from −0.977 to −0.954 V due to the 3D-COOH—COF film and the corresponding corrosion current decreased from 6.31 to 3.98 μA cm^{-2} (Fig. 4i).

3D-COOH—COF protective film significantly promotes the uniform deposition of Zn metal and inhibits the corrosion reactions in aqueous electrolyte, leading to an excellent electrochemical performance. Stripping/plating measurements were carried out in symmetric Zn||Zn cells to validate the role of the COF layer sl at 1 mA cm^{-2} and 1 mA h cm^{-2}. Fig. 5a shows the voltage profile as a function of time. A sudden voltage drop appears after 112 h in the bare Zn cell, signaled by short-circuit because of the growth of Zn dendrites. In contrast, 3D-COOH—COF@Zn shows a very stable cycling for more than 2000 h, which is longer than that (1272 h) of the OH—COF precursor protected Zn foil. It should be mentioned that soft shorts are easy to happen after long-term cycling [42,43]. However, in this study, it is found that the voltage curve is not a line after long-term cycling, indicating that the soft short circuit do not occur. As shown in Fig. S12, the weak diffraction peaks, except for the peaks of pure Zn, can be observed for 3D-COOH—COF@Zn. However, for bare Zn electrode, the strong diffraction peaks are presented owing to the byproduct. These XRD results indicated that 3D-COOH—COF films can effectively protect the zinc electrode and improve the electrochemical performance [44,45]. Additionally, as the current density and areal capacity are further increased to 3 mA cm^{-2} and 3 mA h cm^{-2}, 3D-COOH—COF@Zn shows a minor change of voltage polarization, and a high cycle stability for more

than 1200 h, while the bare Zn foil exhibits a large voltage fluctuation and poor cycling stability (Fig. 5b). It was worth mentioned that 3D-COOH—COF@Zn can be repeatedly plated/stripped over 350 h at 5 mA cm^{-2} and 5 mA h cm^{-2} (Fig. S13a), suggesting the superior performance of the 3D-COOH—COF film in protecting zinc metal. The 3D-COOH—COF film enable a great improvement in terms of cycle stability of Zn foil in aqueous electrolytes, which are better than that of protected Zn anodes reported in the previous studies (Table S2).

The Zn foil morphology after cycling was investigated by SEM, confirming the superior protection effect of 3D-COOH—COF film. As shown in Fig. 5c and S14, the surface of bare Zn after 100 h becomes uneven owing to the serious side reactions, and large amount of "dead" zinc caused by dendrites can be observed after cycling [34,46]. Moreover, the optical photo of the Zn electrode after cycling reveals that the bare Zn is corroded badly (the inset of Fig. 5c). In contrast, SEM image verifies that 3D-COOH—COF protective layer remains smooth and dense without obvious dendrites after the same cycling (Fig. 5d). The corresponding optical photo also further confirms that the 3D-COOH—COF film is very well maintained (the inset of Fig. 5d). The side-view SEM image shows the plating/stripping Zn is located under the 3D-COOH—COF protective layer (Fig. 5e). As displayed in Fig. S15, after 400 h and even 800 h of repeadly plating/stripping of Zn, the 3D-COOH—COF protective film still maintains a good integrity and inhibits the growth of dendrites.

The electrochemical performance of the COF film was further evaluated by the Coulombic efficiency (CE) of Zn plating/stripping, and the half cell of Zn|3D-COOH—COF@Cu and Zn|Cu cells were assembled to test CEs. The Zn|3D-COOH—COF@Cu exhibits excellent cycling performance for more than 1000 cycles, with an average CE as high as above 99.5% (Fig. 5f). In contrast, the Zn|Cu cell fails after only ~70 cycles, and the CE rapidly decreases after 70 cylces. Moreover, the polarization voltage plateau of Zn plating/stripping decreases from ~ 52 to ~ 30 mV from 50th to 1000th cycle underneath the 3D-COOH—COF layer (Fig. 5g) owing to excellent kinetics of Zn^{2+} to pass through the COF layer. Remarkably, the Zn|3D-COOH—COF@Cu cell can cycle stably for over 550 cycles with high efficiency (>99%) even at 3 mA cm^{-2} and 3 mA h cm^{-2} (Fig. S13b). With increasing the current density and the areal specific capacity to 5 mA cm^{-2} and 5 mA h cm^{-2}, the cell with 3D-COOH—COF film can still achieve cycle stability for 350 cycles (Fig. S13c). Such high CE and stability of the Zn|3D-COOH—COF@Cu cell are better than that of previously reported Zn plating/stripping (Table S3).

The performance of the COF-protected Zn as an anode was further investigated in a full cell using MnO_2 as the cathode in 2 M $ZnSO_4$ + 0.1 M $MnSO_4$ electrolyte. Fig. 6a shows the cycling performance of full cells at 1 A g^{-1}. In a cell with a 3D-COOH—COF protected Zn anode, the reversible capacity is 163.61 mA h g^{-1} after 500 cycles at 1 A g^{-1}, with a capacity retention of 78.7% compared to the second cycle. In contrast, the cell with a bare Zn anode delivers a poor electrochemical performance, showing an obvious decrease of the capacity below 32 mA h g^{-1} after 250 cycles. The strong contrast is also reflected by the charge/discharge profiles of the full cells of bare Zn||MnO_2 and 3D-COOH—COF@Zn||MnO_2 cell, which show a lower polarization voltage at the same current rate for the latter (Fig. 6b). Moreover, the full cell of 3D-COOH—COF@Zn||MnO_2 cell also presents a better rate performance, as displayed in Fig. 6c. The surface of the bare Zn was investigated after long-term cycling, showing large amount of dendrites (Fig. 6d), while the 3D-COOH—COF protected Zn anode still maintains a dense and flat surface (Fig. 6e). These results indicate that the 3D-COOH—COF protective layer can significantly reduce the side reactions between the Zn anode and the electrolyte and effectively inhibit the growth of Zn dendrites in the full cells.

3. Conclusions

In summary, we have demonstrated that the rationally designed 3D-COOH—COF films on Zn plates realize the fast and stable Zn electrodeposition. The thin 3D-COOH—COF film has uniform distribution, homogenesous nanochannels, and abundent negative COOH groups, facilitating the Zn^{2+} transport and impeding the pass through of anions. Moreover, the *in-situ* generated COF film significantly reduces the corrosions between metallic Zn and aqueous electrolyte. This novel COF protective film enables the dendrite-free deposition in a symmetric cell over 2000 h at 1 mA cm^{-2} and 1 mA h cm^{-2}. A long-term stable cycling of Zn plating/striping for over 2000 h with an average CE of >99.5% was realized by using 3D-COOH—COF film on the Cu foil. The full cell couped MnO_2 cathode and the COF film protected Zn anode shows an excellent cycling and rate performance. Our finding is important since it provides a simple and effective strategy to stabilize Zn metal, which fundamentally regulates the Zn plating/stripping behavior and has potential to be extend to other akali-metel batteries.

CRediT authorship contribution statement

Kuan Wu: Conceptualization, Methodology, Software, Validation, Formal analysis, Investigation, Writing – original draft, Visualization. **Xiansong Shi:** Conceptualization, Methodology. **Fangfang Yu:** Validation, Formal analysis, Investigation. **Haoxuan Liu:** Data curation, Visualization. **Yuanjun Zhang:** Data curation. **Minghong Wu:** Project administration, Funding acquisition, Formal analysis. **Hua-Kun Liu:** Project administration, Writing – review & editing. **Shi-Xue Dou:** Project administration, Funding acquisition, Writing – review & editing. **Yong Wang:** Resources. **Chao Wu:** Methodology, Resources, Writing – review & editing, Supervision, Project administration, Funding acquisition.

Declaration of Competing Interest

The authors declare that they have no known competing financial interests or personal relationships that could have appeared to influence the work reported in this paper.

Acknowledgements

This work was supported by China Postdoctoral Science Foundation (2020M681260), Science and Technology Commission of Shanghai Municipality (No.20010500400), and Australian Research Council (DP200100365).

Supplementary materials

Supplementary material associated with this article can be found, in the online version, at doi:10.1016/j.ensm.2022.06.032.

References

[1] J. Tarascon, M. Armand, Issues and challenges facing rechargeable lithium batteries, Nature 414 (2001) 359–367, https://doi.org/10.1038/35104644.
[2] E. Fan, L. Li, Zh. Wang, J. Lin, Y. Huang, Y. Yao, R. Chen, F. Wu, Sustainable recycling technology for Li-ion batteries and beyond: challenges and future prospects, Chem. Rev. 120 (2020) 7020–7063, https://doi.org/10.1021/acs.chemrev.9b00535.
[3] X. Liu, H. Euchner, M. Zarrabeitia, X. Gao, G. Elia, A. Groß, S. Passerini, Operando pH measurements decipher H^+/Zn^{2+} intercalation chemistry in high-performance aqueous Zn/δ-V_2O_5 batteries, ACS Energy Lett. 5 (2020) 2979–2986, https://doi.org/10.1021/acsenergylett.0c01767.
[4] Q. Zhang, J. Luan, Y. Tang, X. Ji, H. Wang, Interfacial design of dendrite-free zinc anodes for aqueous zinc-ion batteries, Angew. Chem. Int. Ed. 59 (2020) 13180–13191, https://doi.org/10.1002/anie.202000162.
[5] L. Yuan, J. Hao, C. Kao, C. Wu, H. Liu, S. Dou, S. Qiao, Regulation methods for the Zn/electrolyte interphase and the effectiveness evaluation in aqueous Zn-ion batteries, Energy Environ. Sci. 14 (2021) 5669–5689, https://doi.org/10.1039/d1ee02021h.
[6] L. Zhang, Y. Hou, Recent advances in Zn-ion batteries, Adv. Energy Mater. 11 (2021), 2003823, https://doi.org/10.1002/adfm.201802564.

[7] L. Blanc, D. Kundu, Li. Nazar, Scientific challenges for the implementation of Zn-ion batteries, Joule 4 (2020) 771–799, https://doi.org/10.1016/j.joule.2020.03.002.

[8] C. Xie, Y. Li, D.Sun Q.Wang, Y. Tang, H. Wang, Issues and solutions toward zinc anode in aqueous zinc-ion batteries: a mini review, Carbon Energy 2 (2020) 540–560, https://doi.org/10.1002/cey2.67.

[9] D. Chao, W. Zhou, F. Xie, C. Ye, H. Li, M. Jaroniec, S. Qiao, Roadmap for advanced aqueous batteries: from design of materials to applications, Sci. Adv. 6 (2020) 4098, https://doi.org/10.1126/sciadv.aba4098.

[10] C. Wang, G. Zhu, P. Liu, Q. Chen, Monolithic nanoporous Zn anode for rechargeable alkaline batteries, ACS Nano 14 (2020) 2404–2411, https://doi.org/10.1021/acsnano.9b09669.

[11] Y. Zhang, G. Wang, F. Yu, G. Xu, Z. Li, M. Zhu, Z. Yue, M. Wu, H. Liu, S. Dou, C. Wu, Monolithic nanoporous Zn anode for rechargeable alkaline batteries, Chem. Eng. J. 416 (2021), 128062, https://doi.org/10.1021/acsnano.9b09669.

[12] C. Zhang, W. Shin, L. Zhu, C. Chen, J. Neuefeind, Y. Xu, S. Allec, C. Liu, Z. Wei, A. Daniyar, J. Jiang, C. Fang, P. Greaney, X. Ji, The electrolyte comprising more robust water and superhalides transforms Zn-metal anode reversibly and dendrite-free, Carbon Energy 3 (2021) 339–348, https://doi.org/10.1002/cey2.70.

[13] P. Sun, L. Ma, W. Zhou, M. Qiu, Z. Wang, D. Chao, W. Mai, Simultaneous regulation on solvation shell and electrode interface for dendrite-free Zn ion batteries achieved by a low-cost glucose additive, Angew. Chem. Int. Ed. 60 (2021) 18247–18255, https://doi.org/10.1002/anie.202105756.

[14] C. Liu, X. Xie, B. Lu, J. Zhou, S. Liang, Electrolyte strategies toward better zinc-ion batteries, ACS Energy Lett. 6 (2021) 1015–1033, https://doi.org/10.1021/acsenergylett.0c02684.

[15] C. Li, R. Kingsbury, L. Zhou, A. Shyamsunder, K. Persson, Linda. Nazar, Tuning the solvation structure in aqueous zinc batteries to maximize Zn-ion intercalation and optimize dendrite-free zinc plating, ACS Energy Lett. 7 (2022) 533–540, https://doi.org/10.1021/acsenergylett.1c02514.

[16] Y. Zhang, Z. Huang, K. Wu, F. Yu, M. Zhu, G. Wang, G. Xu, M. Wu, H. Liu, S. Dou, C. Wu, 2D anionic nanosheet additive for stable Zn metal anodes in aqueous electrolyte, Chem. Eng. J. 430 (2022), 133042, https://doi.org/10.1016/j.cej.2021.133042.

[17] F. Xie, H. Li, X. Wang, X. Zhi, D. Chao, K. Davey, S. Qiao, Mechanism for zincophilic sites on zinc-metal anode hosts in aqueous batteries, Adv. Energy Mater. 11 (2021), 2003419, https://doi.org/10.1002/aenm.202003419.

[18] L. Kang, M. Cui, F. Jiang, Y. Gao, H. Luo, J. Liu, W. Liang, C. Zhi, Nanoporous $CaCO_3$ coatings enabled uniform Zn stripping/plating for long-life zinc rechargeable aqueous batteries, Adv. Energy Mater. 8 (2018), 1801090, https://doi.org/10.1002/aenm.201801090.

[19] N. Zhang, S. Huang, Z. Yuan, J. Zhu, Z. Zhao, Z. Niu, Direct self-assembly of MXene on Zn anodes for dendrite-free aqueous zinc-ion batteries, Angew. Chem. Int. Ed. 60 (2021) 2861–2865, https://doi.org/10.1002/anie.202012322.

[20] Y. Zhang, M. Zhu, G. Wang, F. Du, F. Yu, K. Wu, M. Wu, S. Dou, H. Liu, C. Wu, Dendrites-free Zn metal anodes enabled by an artificial protective layer filled with 2D anionic nanosheets, Small Methods 5 (2021), 2100650, https://doi.org/10.1002/smtd.202100650.

[21] J. Han, H. Euchner, M. Kuenzel, S. Hosseini, A. Groß, A. Varzi, S. Passerini, A thin and uniform fluoride-based artificial interphase for the zinc metal anode enabling reversible Zn/MnO_2 batteries, ACS Energy Lett. 6 (2021) 3063–3071, https://doi.org/10.1021/acsenergylett.1c01249.

[22] J. Hao, X. Li, S. Zhang, F. Yang, X. Zeng, S. Zhang, G. Bo, C. Wang, Z. Guo, Designing dendrite-free zinc anodes for advanced aqueous zinc batteries, Adv. Funct. Mater. (2020), 2001263, https://doi.org/10.1002/adfm.202001263.

[23] Y. Yang, C. Liu, Z. Lv, H. Yang, Y. Zhang, M. Ye, L. Chen, J. Zhao, C. Li, Synergistic manipulation of Zn2+ ion flux and desolvation effect enabled by anodic growth of a 3D ZnF_2 matrix for long-lifespan and dendrite-free Zn metal anodes, Adv. Mater. 33 (2021), 2007388, https://doi.org/10.1002/adma.202007388.

[24] D. Li, L. Cao, T. Deng, S. Liu, C. Wang, Design of a solid electrolyte interphase for aqueous Zn batteries, Angew. Chem. Int. Ed. 60 (2021) 13035–13041, https://doi.org/10.1002/anie.202103390.

[25] L. Cao, D. Li, T. Deng, Q. Li, C. Wang, Hydrophobic organic electrolyte protected Zn anodes for aqueous Zn batteries, Angew. Chem. Int. Ed. 59 (2020) 19292–19296, https://doi.org/10.1002/anie.202008634.

[26] X. Shi, Z. Zhang, S. Fang, J. Wang, Y. Zhang, Y. Wang, Flexible and robust three-dimensional covalent organic framework membranes for precise separations under extreme conditions, Nano Lett. 21 (2021) 8355–8362, https://doi.org/10.1021/acs.nanolett.1c02919.

[27] Q. Lu, Y. Ma, H. Li, X. Guan, Y. Yusran, M. Xue, Q. Fang, Y. Yan, S. Qiu, V. Valtchev, Postsynthetic functionalization of three-dimensional covalent organic framework for selective extraction of lanthanide ions, Angew. Chem. Int. Ed. 57 (2018) 6042–6048, https://doi.org/10.1002/anie.201712246.

[28] X. Guan, F. Chen, Q. Fang, S. Qiu, Design and applications of three dimensional covalent organic frameworks, Chem. Soc. Rev. 49 (2020) 1357, https://doi.org/10.1039/c9cs00911f.

[29] P. Cao, X. Zhou, A. Wei, Q. Meng, H. Ye, W. Liu, J. Tang, J. Yang, Fast-charging and ultrahigh-capacity zinc metal anode for high-performance aqueous zinc-ion batteries, Adv. Funct. Mater. (2021), 2100398, https://doi.org/10.1002/adfm.202100398.

[30] Z. Zhao, R. Wang, C. Peng, W. Chen, T. Wu, B. Hu, W. Weng, Y. Yao, J. Zeng, Z. Chen, P. Liu, Y. Liu, G. Li, J. Guo, H. Lu, Z. Guo, Horizontally arranged zinc platelet electrodeposits modulated by fluorinated covalent organic framework film for high-rate and durable aqueous zinc ion batteries, Nat. Commun. 12 (2021) 6606, https://doi.org/10.1038/s41467-021-26947-9.

[31] Y. Wang, C. Wang, Z. Ni, Y. Gu, B. Wang, Z. Guo, Z. Wang, D. Bin, J. Ma, Y. Wang, Binding zinc ions by carboxyl groups from adjacent molecules toward long-life aqueous zinc-organic batteries, Adv. Mater. 32 (2020), 2000338, https://doi.org/10.1002/adma.202000338.

[32] D. Briggs, XPS studies of polymer surface modifications and adhesion mechanisms, J. Adhes. 13 (1982) 287–301, https://doi.org/10.1080/00218468208073192.

[33] X. Liu, F. Yang, W. Xu, Y. Zeng, J. He, X. Lu, Zeolitic imidazolate frameworks as Zn^{2+} modulation layers to enable dendrite-free Zn anodes, Adv. Sci. 7 (2020), 2002173, https://doi.org/10.1002/advs.202002173.

[34] X. Zeng, J. Mao, J. Hao, J. Liu, S. Liu, Z. Wang, Y. Wang, S. Zhang, T. Zheng, J. Liu, P. Rao, Z. Guo, Electrolyte design for *in situ* construction of highly Zn^{2+}-conductive solid electrolyte interphase to enable high-performance aqueous zn-ion batteries under practical conditions, Adv. Mater. 33 (2021), 2007416, https://doi.org/10.1002/adma.202007416.

[35] L. Zhang, Y. Hou, Comprehensive analyses of aqueous Zn metal batteries: characterization methods, simulations, and theoretical calculations, Adv. Energy Mater. 11 (2021), 2003823, https://doi.org/10.1002/aenm.202003823.

[36] Q. Yang, Q. Li, Z. Liu, D. Wang, Y. Guo, X. Li, Y. Tang, H. Li, B. Dong, C. Zhi, Dendrites in Zn-based batteries, Adv. Mater. 32 (2020), 2001854, https://doi.org/10.1002/adma.202001854.

[37] L. Zhang, B. Zhang, T. Zhang, T. Li, T. Shi, W. Li, T. Shen, X. Huang, J. Xu, X. Zhang, Z. Wang, Y. Hou, Eliminating dendrites and side reactions via a multifunctional ZnSe protective layer toward advanced aqueous Zn metal batteries, Adv. Funct. Mater. (2021), 2100186, https://doi.org/10.1002/adfm.202100186.

[38] J. Hao, B. Li, X. Li, X. Zeng, S. Zhang, F. Yang, S. Liu, D. Li, C. Wu, Z. Guo, An in-depth study of Zn metal surface chemistry for advanced aqueous Zn-ion batteries, Adv. Mater. 32 (2020), 2003021, https://doi.org/10.1002/adma.202003021.

[39] Q. Zhang, J. Luan, L. Fu, S. Wu, Y. Tang, X. Ji, H. Wang, The three-dimensional dendrite-free zinc anode on a copper mesh with a zinc-oriented polyacrylamide electrolyte additive, Angew. Chem. Int. Ed. 131 (2019) 15988–15994, https://doi.org/10.1002/anie.201907830.

[40] H. Yan, S. Li, Y. Nan, S. Yang, B. Li, Ultrafast zinc–ion–conductor interface toward high-rate and stable zinc metal batteries, Adv. Energy Mater. (2021), 2100186, https://doi.org/10.1002/aenm.202100186.

[41] M. Rosso, T. Gobron, C. Brissot, J. Chazalviel, S. Lascaud, Onset of dendritic growth in lithium/polymer cells, J. Power Sources 804 (2001) 97–98, https://doi.org/10.1016/S0378-7753(01)00734-0.

[42] Q. Li, A. Chen, D. Wang, Z. Pei, C. Zhi, Soft Shorts" hidden in zinc metal anode research, Joule 6 (2022) 273–279, https://doi.org/10.1016/j.joule.2021.12.009.

[43] D. Wang, Q. Li, Y. Zhao, H. Hong, H. Li, Z. Huang, G. Liang, Q. Yang, C. Zhi, Insight on organic molecules in aqueous Zn-ion batteries with an emphasis on the Zn anode regulation, Adv. Energy Mater. 12 (2022), 2102707, https://doi.org/10.1002/aenm.202102707.

[44] J. Hao, L. Yuan, C. Ye, D. Chao, K. Davey, Z. Guo, S. Qiao, Boosting zinc electrode reversibility in aqueous electrolytes by using low-cost antisolvents, Angew. Chem. Int. Ed. 60 (2021) 7366–7375, https://doi.org/10.1002/anie.202016531.

[45] J. Hao, X. Li, X. Zeng, D. Li, J. Mao, Z. Guo, Deeply understanding the Zn anode behavior and corresponding improvement strategies in different aqueous Zn-based batteries, Energy Environ. Sci. 13 (2020) 3917–3949, https://doi.org/10.1039/d0ee02162h.

[46] Y. Zhang, M. Zhu, K. Wu, F. Yu, G. Wang, G. Xu, M. Wu, H. Liu, S. Dou, C. Wu, An in-depth insight of a highly reversible and dendrite-free Zn metal anode in an hybrid electrolyte, J. Mater. Chem. A 9 (2021) 4253, https://doi.org/10.1039/d0ta11668h.